Aalborg Universitet

AALBORG UNIVERSITY
DENMARK

Measurement-based Double-Directional Polarimetric Characterization of Outdoor Massive MIMO Propagation Channels at 3.5GHz

Hao, Le; Rodríguez-Piñeiro, José ; Cai, Xuesong; Yin, Xuefeng; Hong, Jingxiang ; Pedersen, Gert Frølund; Schwarz, Stefan

Published in:
IEEE 21st International Workshop on Signal Processing Advances in Wireless Communications (SPAWC)

DOI (link to publication from Publisher):
10.1109/SPAWC48557.2020.9154274

Publication date:
2020

Document Version
Accepted author manuscript, peer reviewed version

Link to publication from Aalborg University

Citation for published version (APA):
Hao, L., Rodríguez-Piñeiro, J., Cai, X., Yin, X., Hong, J., Pedersen, G. F., & Schwarz, S. (2020). Measurement-based Double-Directional Polarimetric Characterization of Outdoor Massive MIMO Propagation Channels at 3.5GHz. In *IEEE 21st International Workshop on Signal Processing Advances in Wireless Communications (SPAWC)* [9154274] IEEE. IEEE International Workshop on Signal Processing Advances in Wireless Communications (SPAWC) https://doi.org/10.1109/SPAWC48557.2020.9154274

General rights
Copyright and moral rights for the publications made accessible in the public portal are retained by the authors and/or other copyright owners and it is a condition of accessing publications that users recognise and abide by the legal requirements associated with these rights.

? Users may download and print one copy of any publication from the public portal for the purpose of private study or research.
? You may not further distribute the material or use it for any profit-making activity or commercial gain
? You may freely distribute the URL identifying the publication in the public portal ?

Take down policy
If you believe that this document breaches copyright please contact us at vbn@aub.aau.dk providing details, and we will remove access to the work immediately and investigate your claim.

Measurement-based Double-Directional Polarimetric Characterization of Outdoor Massive MIMO Propagation Channels at 3.5 GHz

Le Hao[1], José Rodríguez-Piñeiro[1], Xuesong Cai[2], Xuefeng Yin[1,4], Jingxiang Hong[1], Gert Frølund Pedersen[2], and Stefan Schwarz[3]

[1]College of Electronics and Information Engineering, Tongji University, Shanghai, China
[2]Department of Electronic Systems, Aalborg University, Aalborg, 9220, Denmark
[3]Christian Doppler Laboratory for Dependable Wireless Connectivity for the Society in Motion, TU Wien, Vienna, Austria
[4]National Computer and Inf. Technology Practical Education Demonstration Center, Tongji University, Shanghai, China
Email:[1]{haole, j.rpineiro, hongjx, yinxuefeng}@tongji.edu.cn, [2]{xuc,gfp}@es.aau.dk, [3]sschwarz@nt.tuwien.ac.at

***Abstract*—Massive multiple-input multiple-output (MIMO) is a key technology for 5G wireless communications since it can improve network throughput, capacity, spatial efficiency, etc. utilizing large-scale antenna arrays. In this paper, we study the direction of departure (DOD) and direction of arrival (DOA) power spectra and the angular spreads for suburban line-of-sight (LoS) environment. Our study is based on a measurement campaign conducted at a carrier frequency of 3.5 GHz, with a bandwidth of 160 MHz and $\pm 45^\circ$ dual-polarized 4×8 planar and cylindrical antenna arrays at the transmitter and the receiver, respectively. The space-alternating generalized expectation-maximization (SAGE) algorithm is applied to jointly estimate the DOA, DOD, delay and complex amplitude of the propagation channel measured by the massive MIMO system. Results show that the double-directional channel characteristics exhibit dependence with the employed polarization combination. The obtained characterization results are of great value for the analysis of polarization-dependent design and antenna selection strategies for MIMO systems.**

***Index Terms*—Massive MIMO, large-scale antenna array, channel characteristics and polarization.**

I. Introduction

With rapidly increasing demands for higher data rate, capacity, and coverage, the research on the fifth generation (5G) mobile communication system is still a hot topic [1]. Massive multiple-input multiple-output (MIMO), as one of the innovative technologies in 5G wireless communication systems [2], is considered to be an enabler for the development of broadband (fixed and mobile) networks, which offers huge advantages in terms of reliability, security, robustness, energy efficiency, and spectral efficiency [3].

As a foundation for any wireless communication, the research on propagation channels is of great significance for the design, performance evaluation, and improvement of massive MIMO systems [4]. In recent years, massive MIMO propagation channel characterization and modeling have attracted much attention in both academia and industry. For instance, the authors in [5] proved the feasibility and reasonability of the virtual measurement with a virtual 256-element uniform planar array through a comparison between virtual and practical measurement. Spatial characteristics in elevation domain for 3D MIMO wideband channel were analyzed and modeled in [6] based on the measurements at 3.5 GHz. In addition, massive MIMO propagation characteristics including the power delay profile, delay spread and angular parameters were studied in [7] via the space-alternating generalized expectation-maximization (SAGE) algorithm, which are based on measurements in a Urban Macro-cell (UMa) Scenario at 3.5 and 6 GHz. Nevertheless, appropriate channel models for massive MIMO are still limited. To promote massive MIMO techniques from theory to practice, more characterizations for massive MIMO channel in different scenarios are needed.

In this paper, we continue with our earlier contributions [8], [9], with a focus on the polarization and angular domain characteristics for the massive MIMO channel. Since the transmitter (Tx) and receiver (Rx) antenna elements have both $+45^\circ$ and -45° polarizations, we choose Tx and Rx antenna pairs with the same or different polarization combinations, such as Tx $+45^\circ$ with Rx $+45^\circ$, Tx $+45^\circ$ with Rx -45°, Tx -45° with Rx $+45^\circ$, and Tx -45° with Rx -45°, to analyze the channel polarimetric characteristics. Futhermore, we apply the Bartlett beamforming method [10] to estimate the power angular spectrum (PAS). Then the results are compared with the reconstructed power spectrum by the SAGE algorithm.

The rest of this paper is organized as follows. In Sect. II, the measurement environment and equipment are introduced. In Sect. III, the Bartlett beamforming and SAGE algorithm are introduced to estimate the PAS and angular spread. Results and discussions are presented in Sect. IV. Finally, conclusions are drawn in Sect. V.

II. Channel Measurement

The measurement campaign was conducted in a suburban road of Shanghai Jiaotong University, China. The center frequency was 3.5 GHz, and the bandwidth was 160 MHz. Fig. 1(a) depicts the measurement environment, and Fig. 1(b) illustrates

the measurement setup used at the Rx side. The base station (BS) equipped with a 4×8 planar patch antenna array (see Fig. 2(a)) was fixed at the top of a building with a height of 16 meters. The user equipment (UE), which includes a cylindrical structure with 8 columns of 1×4 patch antenna arrays (see Fig. 3), was set on a 1.8-meter-high trolley and located at the center of a crossroad. Both the locations of BS and UE are marked in the map in Fig. 1(a). The channel between the Tx and Rx antennas can be regarded as LoS scenario. The Tx antenna patches are the same as Rx, and each antenna element contains two RF output ports with polarizations of $+45^\circ$ and -45°, respectively. Fig. 2(b) illustrates the polarization of Tx and Rx antenna patches.

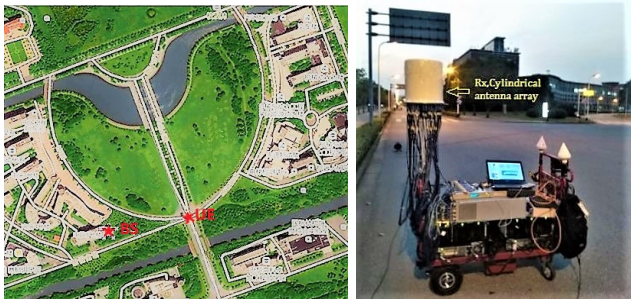

(a) (b)

Fig. 1. (a) Measurement environment. (b) Setup used at Rx side.

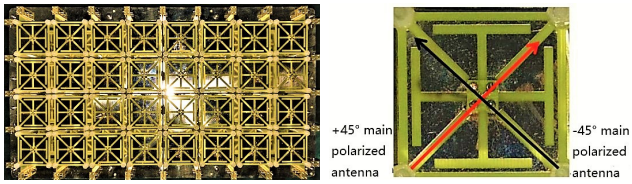

(a) (b)

Fig. 2. (a) Tx antenna array. (b) Polarizations of Tx and Rx antenna elements.

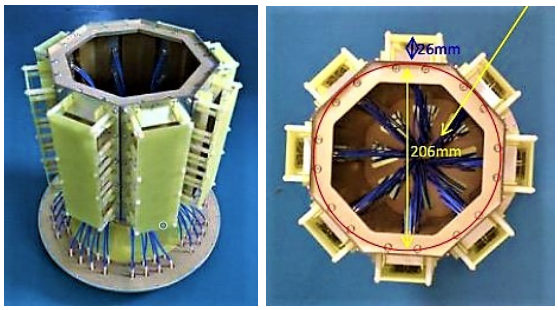

(a) (b)

Fig. 3. Rx antenna array: (a) Side view; (b) Top view.

III. Data Processing

The channel impulse responses (CIRs) of the scenario of interest were obtained from measurements. In our case, the measurement was repeated for 4 times, each with 1023 delay samples. The subsequent data processing is based on the average of the 4 cycles measurement data, in order to enhance the signal to noise ratio (SNR). Since each Tx and Rx antenna elements have two polarizations, there are 64×64 sub-channels in total. It is worth noting that the dimensions of the channel parameters that a channel estimation technique can resolve are highly dependent on the characteristics of the antenna arrays: their geometrical structure, the array radiation patterns, and the polarizations [11].

A. Power Angular Spectrum

Firstly, the Bartlett beamforming method is applied to estimating the PAS, i.e., direction of departure (DOD) and direction of arrival (DOA) power spectra, from the original CIRs obtained from measurements. The application of this method is based on the assumption that the array response, the so-called steering vector $\boldsymbol{c}(\theta,\phi)$ evaluated at the direction with azimuth ϕ and elevation θ, is known. Here we only give the final expressions for calculating the PAS as follows. More details of the algorithm can be found in [10].

For a given $\boldsymbol{c}(\theta,\phi)$, the PAS can be computed as

$$p(\theta,\phi)=\frac{\boldsymbol{c}(\theta,\phi)^{\mathrm{H}}\widehat{\boldsymbol{R}}\boldsymbol{c}(\theta,\phi)}{\boldsymbol{c}(\theta,\phi)^{\mathrm{H}}\boldsymbol{c}(\theta,\phi)}, \tag{1}$$

where $(\cdot)^{\mathrm{H}}$ indicates the Hermitian of the matrix, and $\widehat{\boldsymbol{R}}$ is the estimated covariance matrix of the received signal. For a double-directional MIMO system, the PAS calculation can be extended as

$$p(\theta_{\mathrm{T}},\phi_{\mathrm{T}},\theta_{\mathrm{R}},\phi_{\mathrm{R}})=\frac{\boldsymbol{D}^{\mathrm{H}}\widehat{\boldsymbol{R}}\boldsymbol{D}}{\boldsymbol{D}^{\mathrm{H}}\boldsymbol{D}}, \tag{2}$$

with $\boldsymbol{D}=[\boldsymbol{c}_{\mathrm{T}}(\theta_{\mathrm{T}},\phi_{\mathrm{T}})\otimes\boldsymbol{c}_{\mathrm{R}}(\theta_{\mathrm{R}},\phi_{\mathrm{R}})]$, and

$$\widehat{\boldsymbol{R}}=\frac{1}{\mathrm{NM}}\sum_{k=1}^{K}\mathrm{vec}[\mathrm{Y}(k)]\mathrm{vec}[\mathrm{Y}(k)]^{\mathrm{H}}, \tag{3}$$

where $\otimes$ is the Kronecker product, $\mathrm{Y}(k)\in\mathbb{C}^{N\times M}$ indicates the received signal at the k-th delay bin with M and N as the number of Tx and Rx antennas, respectively, and $\mathrm{vec}[\cdot]$ is the vectorization operator, which sequentially stacks the columns of a matrix into a single column vector. By conducting the marginal operation, we obtain PAS for different angle parameters, e.g.

$$p(\theta_{\mathrm{T}})=\iiint p(\theta_{\mathrm{T}},\phi_{\mathrm{T}},\theta_{\mathrm{R}},\phi_{\mathrm{R}})d\theta_{\mathrm{R}}\phi_{\mathrm{R}}d\phi_{\mathrm{T}}, \tag{4}$$

and PAS for other parameters, i.e. $p(\theta_{\mathrm{R}})$, $p(\phi_{\mathrm{T}})$,$p(\phi_{\mathrm{R}})$, can be calculated similarly.

B. Angular Spread

Angular spread is a power-weighted spatial parameter widely used to characterize the angular dispersion of power departure/arrival. The angular spread is defined as the second order moment of the PAS [12], which can be calculated as:

$$\mathrm{AS}_{\psi}=\sqrt{\frac{\sum_{\psi=\psi_{\min}}^{\psi_{\max}}|\exp(j\psi)-\mu_{\psi}|^2\cdot p(\psi)}{\sum_{\psi=\psi_{\min}}^{\psi_{\max}}p(\psi)}}, \tag{5}$$

where

$$\mu_\psi = \frac{\sum_{\psi=\psi_{\min}}^{\psi_{\max}} \exp(j\psi)\cdot p(\psi)}{\sum_{\psi=\psi_{\min}}^{\psi_{\max}} p(\psi)}, \tag{6}$$

is the mean value of the angle ψ. $p(\psi)$ is the power at the angle of ψ, and ψ is the angle (either $\theta_{\mathrm{T}}, \phi_{\mathrm{T}}, \theta_{\mathrm{R}}, \phi_{\mathrm{R}}$) given in radians. The range of elevation is $\theta \in [0, 180)$, and the azimuth range is $\phi \in [-180, 180)$.

C. Multipath Channel Parameters

The well-known SAGE algorithm can be used to jointly estimate the multipath channel parameters from the CIR [13]. In particular, for the double-directional MIMO channel, the SAGE algorithm is applied to jointly estimate the DOA and the DOD of the Multi-Path Components (MPCs). If we consider an overall angle distribution, the azimuth angles and elevation angles of the estimated Multi-Path Components (MPCs) for all the Tx/Rx antennas are combined together. Hence, in order to account for the double-directional propagation for the MIMO system, the DOD and DOA should be estimated simultaneously. The underlying signal model for the MIMO channel (including noise) can be formatted as

$$\mathbf{h}(t,\tau) = \sum_{l=1}^{L} \mathbf{C}_{\mathrm{R}}(\mathbf{\Omega}_{\mathrm{R}}^l) \begin{pmatrix} \alpha^l_{(+,+)} & \alpha^l_{(+,-)} \\ \alpha^l_{(-,+)} & \alpha^l_{(-,-)} \end{pmatrix} \mathbf{C}_{\mathrm{T}}(\mathbf{\Omega}_{\mathrm{T}}^l)^{\mathrm{T}} \cdot \exp\{j2\pi\nu^l t\}\delta(t-\tau^l) + \mathbf{W}, \tag{7}$$

for $t \in [0, T)$, where T is the measurement duration (or observation time). In (7), L denotes the total number of propagation paths, whereas τ^l and ν^l represent the delay and Doppler frequency of the l-th path, respectively. $\alpha^l_{(p_{\mathrm{T}},p_{\mathrm{R}})}$ is the complex attenuation factor for the l-th path, where $p_{\mathrm{R}}, p_{\mathrm{T}} \in \{+,-\}$ denote the polarizations used at the receiver and the transmitter, respectively. In order to alleviate the notation, "+" is used to denote the $+45°$ polarization and "−" for the $-45°$ one[1]. $\mathbf{C}_{\mathrm{R}}(\mathbf{\Omega}_{\mathrm{R}}^l) \in \mathbb{C}^{M\times 2}$ is a matrix containing the steering vectors of the receiver array for the $\pm 45°$ polarizations, which depend on the DOA, defined as $\mathbf{\Omega}_{\mathrm{R}}^l = (\theta_{\mathrm{R}}^l, \phi_{\mathrm{R}}^l)$, being θ_{R}^l the elevation of arrival (EOA) and ϕ_{R}^l the azimuth of arrival (AOA) for the l-th path. Similarly, $\mathbf{C}_{\mathrm{T}}(\mathbf{\Omega}_{\mathrm{T}}^l) \in \mathbb{C}^{M\times 2}$ is a matrix containing the steering vectors of the receiver array for the $\pm 45°$ polarizations, which depend on the DOD, defined as $\mathbf{\Omega}_{\mathrm{T}}^l = (\theta_{\mathrm{T}}^l, \phi_{\mathrm{T}}^l)$, being θ_{T}^l the elevation of departure (EOD) and ϕ_{T}^l the azimuth of departure (AOD) for the l-th path. Finally, $\delta(t)$ is the impulse response (Dirac Delta function) and $\mathbf{W} \in \mathbb{C}^{N\times M}$ is a matrix whose elements are Gaussian-distributed, in order to account for the contribution of the noise.

[1]Note that a common complex attenuation factor is considered for all the antennas at the transmitter and receiver arrays, since the experimental results are obtained in far-field conditions.

IV. Results Analysis

A. Power Angular Spectrum

The normalized PAS for DOD and DOA, which are estimated by Bartlett beamforming from the original measured CIRs, are shown in Fig. 4 and Fig. 5, respectively. From these figures, we can observe that the main departure direction is at the elevation of $90°$ and azimuth of $-100°$. It is obvious that the array response may have a signifcant impact on the estimated power spectrum. For the four different polarization combinations, the DOD power spectrums have no big differences regarding the main beam direction. However, when the Tx and Rx antenna arrays are cross-polarized, the powers are much higher than when they are co-polarized. In the cross-polarization cases, the highest normalized power can be 1, but in the co-polarized cases, the highest power is 0.26 in linear scale.

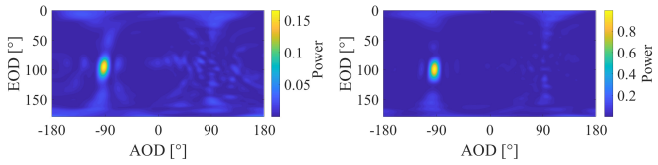

(a) $Tx+45°, Rx+45°$ (b) $Tx-45°, Rx+45°$

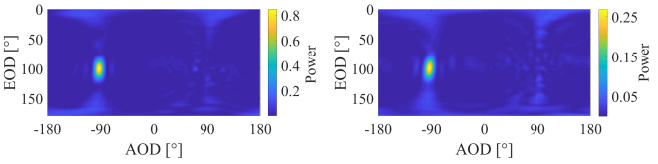

(c) $Tx+45°, Rx-45°$ (d) $Tx-45°, Rx-45°$

Fig. 4. PAS at departure side (DOD).

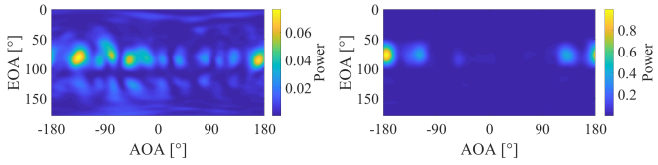

(a) $Tx+45°, Rx+45°$ (b) $Tx-45°, Rx+45°$

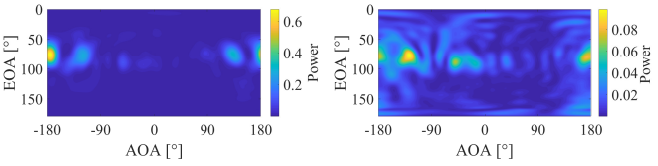

(c) $Tx+45°, Rx-45°$ (d) $Tx-45°, Rx-45°$

Fig. 5. PAS at arrival side (DOA).

Regarding the DOA power spectrum, it can be also observed that the power values in cross-polarization cases are higher than those for co-polarization, being the difference about 0.9 in linear scale. Moreover, the power spectrum for the two cross-polarization cases is similar. Similarities are also found for the two co-polarization cases. Furthermore, when the Tx and Rx antennas are cross-polarized, the powers are more concentrated around the elevation of $75°$ and azimuth of $-175°$. However, when the Tx and Rx antennas are co-polarized, the power spreads more, being distributed for all

azimuth angles at the main elevation of 75°. The detailed explanation for the effects of different polarizations is given in our previous contribution [8]. Due to the same antenna structure, when the Tx and Rx antennas are pointing to each other, the transmitted $-45°$ polarized signal matches the $+45°$ polarized Rx antenna port. When they are pointing to the same direction, the transmitted $-45°$ polarized signal comes to the $-45°$ polarized Rx antenna port.

B. Angular Spread

The angular spreads for both DOD and DOA are shown in Fig. 6. Fig. 6(a) and (b) depict the EOD and AOD spreads, respectively. From these two figures we can observe that when the azimuth is $-93°$, the EOD spreads have a deep valley. When the elevation is $100°$, the AOD spreads have a deep valley, which is coherent with the PAS in Fig. 4. This means that the power is concentrated around $-100°$ azimuth and $100°$ elevation. Generally speaking, the AOD spreads are larger than EOD spreads. In addition, the angular spreads exhibit no much dependency with the polarization.

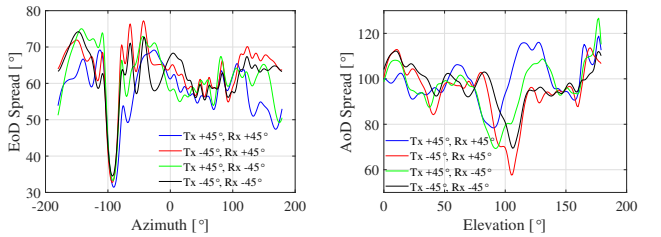

(a) Angular spread for EOD seen at each AOD angle. (b) Angular spread for AOD seen at each EOD angle.

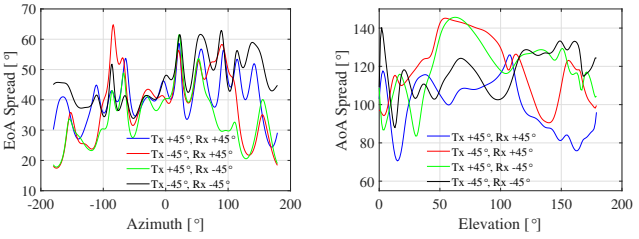

(c) Angular spread for EOA seen at each AOA angle. (d) Angular spread for AOA seen at each EOA angle.

Fig. 6. Angular spread for DOD and DOA w.r.t polarization combination.

Similar observations can be observed at the DOA side. E.g., the AOA spreads are larger than the EOA spreads in general and the polarization does not effect the angular spread very much. Since the power distribution in this case is more disperse, the angular spreads also exhibit big fluctuations. However, the maximum power concentration can be found for $15°$ elevation and $\pm 180°$ azimuth.

C. Reconstructed Channel Parameters via SAGE

By using the SAGE algorithm, the channel parameters such as amplitude, delay, EOD, AOD, EOA, and AOA are estimated. The estimated channel is reconstructed from those estimated parameters, by applying equation (7). During the procedure of running SAGE, 10 paths are estimated, and convergence is achieved after executing 4 iterations[2]. The obtained PASs at both DOD and DOA sides are shown in Figs. 7 and 8, respectively. From these figures, we can find that the reconstructed PAS at DOD side is very close to the original PAS in Fig. 4 except for some of the side beams, which are stronger than the original ones. The same phenomenon can be observed w.r.t the polarization and main beam direction.

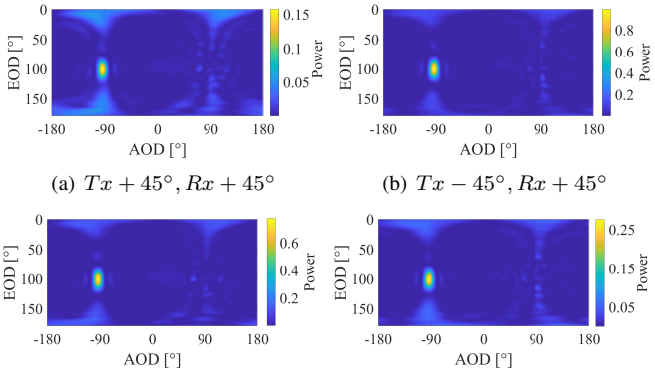

(a) $Tx + 45°, Rx + 45°$ (b) $Tx - 45°, Rx + 45°$

(c) $Tx + 45°, Rx - 45°$ (d) $Tx - 45°, Rx - 45°$

Fig. 7. Reconstructed PAS at departure side (DOD).

From Fig. 8, we can observe that the reconstructed PAS at DOA side is also very similar to the original PAS in Fig. 5, especially for the two cross-polarization cases. However, for the two co-polarization cases, the reconstructed PAS reproduces two main beams at the elevation of $75°$ and the azimuths of $-145°$ and $180°$. It cannot restore some strong side beams seen in Fig. 5. For example, the original side beams at azimuth of $-50°$ are stronger than the reconstructed ones. In fact, due to lower SNR, some weak components cannot be extracted precisely.

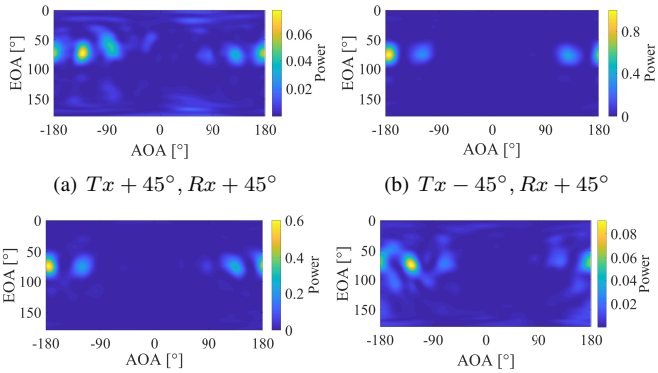

(a) $Tx + 45°, Rx + 45°$ (b) $Tx - 45°, Rx + 45°$

(c) $Tx + 45°, Rx - 45°$ (d) $Tx - 45°, Rx - 45°$

Fig. 8. Reconstructed PAS at arrival side (DOA).

In order to study the detailed information of delay, power, and directions from the estimated paths, the power angle delay profiles (PADPs) of both DOD and DOA are drawn in Fig. 9 and Fig. 10, respectively. The X and Y coordinates denote the azimuth and elevation angles, respectively. Each dot represents a single MPC, being the delay value indicated by the dot color, whereas the dot size accounts for the power value, the larger

[2]For details on the SAGE algorithm, we refer the reader to [13].

size means the higher power. We checked that $L = 10$ paths can capture most of the energy of the channel. From Fig. 9, we can observe that most of the paths depart at an elevation of around 100° and azimuths of around -100° and 100°, whereas the arrival angles concentrate mostly at the elevation of 75° and azimuths of -175° and 175°, as shown in Fig. 10. The directions are similar for both co-polarization cases, as well as they are for both cross-polarization ones. However, there are clear differences between the co-polarization and the cross-polarization cases. For example, the paths are more concentrated to one direction in the cross-polarization cases, but more disperse in the co-polarization cases.

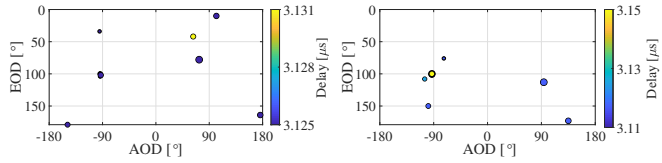

(a) $Tx + 45^\circ, Rx + 45^\circ$ (b) $Tx - 45^\circ, Rx + 45^\circ$

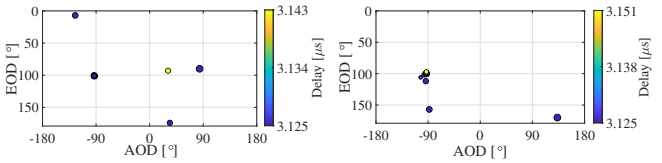

(c) $Tx + 45^\circ, Rx - 45^\circ$ (d) $Tx - 45^\circ, Rx - 45^\circ$

Fig. 9. PADP at departure side (DOD).

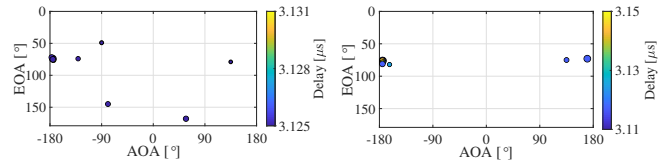

(a) $Tx + 45^\circ, Rx + 45^\circ$ (b) $Tx - 45^\circ, Rx + 45^\circ$

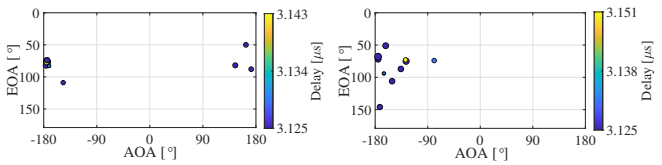

(c) $Tx + 45^\circ, Rx - 45^\circ$ (d) $Tx - 45^\circ, Rx - 45^\circ$

Fig. 10. PADP at arrival side (DOA).

V. Conclusions

Based on a massive MIMO measurement campaign at the frequency of 3.5 GHz in a suburban LoS scenario, this paper analyzes the PAS and angular spread, as well as the MPC channel parameters such as amplitude, delay, EOD, AOD, EOA and AOA. Results show that channel characteristics are heavily dependent on the antenna structures and polarizations. For example, the departure and arrival angular characteristics (PAS and angular spread) are very different between them when different antenna arrays are used at Tx and Rx sides. The PAS for co-polarization cases is different from that for cross-polarization, but it is similar between the two co-polarization cases, and also close for the two cross-polarization cases. Furthermore, the SAGE algorithm was used, and the results reveal the constellation of the MPCs. Collectively, these results shed light on the design of massive MIMO system in outdoor environments.

Acknowledgment

This work was partially supported by the National Natural Science Foundation of China (Grants No. 61850410529 and 61971313).

References

[1] B. Ai, K. Guan, M. Rupp, T. Kurner, X. Cheng, X. Yin, Q. Wang, G. Ma, Y. Li, L. Xiong, and J. Ding, "Future railway services-oriented mobile communications network," *IEEE Communications Magazine*, vol. 53, no. 10, pp. 78–85, October 2015.

[2] J. Chen, X. Yin, and S. Wang, "Measurement-based massive MIMO channel modeling in 13-17 GHz for indoor hall scenarios," in *IEEE International Conference on Communications (ICC)*, Chengdu, China, May 2016, pp. 1–5.

[3] K. N. R. S. V. Prasad, E. Hossain, and V. K. Bhargava, "Energy Efficiency in Massive MIMO-Based 5G Networks: Opportunities and Challenges," *IEEE Wireless Communications*, vol. 24, no. 3, pp. 86–94, June 2017.

[4] R. He, B. Ai, G. Wang, K. Guan, Z. Zhong, A. F. Molisch, C. Briso-Rodriguez, and C. P. Oestges, "High-Speed Railway Communications: From GSM-R to LTE-R," *IEEE Vehicular Technology Magazine*, vol. 11, no. 3, pp. 49–58, Sep. 2016.

[5] Hao Yu, J. Zhang, Qingfang Zheng, Zhe Zheng, Lei Tian, and Ye Wu, "The rationality analysis of massive MIMO virtual measurement at 3.5 GHz," in *2016 IEEE/CIC International Conference on Communications in China (ICCC Workshops)*, July 2016, pp. 1–5.

[6] L. Tian, J. Zhang, Y. Zhang, and Y. Zheng, "Spatial Characteristics of 3D MIMO Wideband Channel in Indoor Hotspot Scenario at 3.5 GHz," in *2018 IEEE/CIC International Conference on Communications in China (ICCC)*, Aug 2018, pp. 752–756.

[7] Z. Zheng, J. Zhang, Y. Yu, L. Tian, and Y. Wu, "Propagation characteristics of massive MIMO measurements in a UMa scenario at 3.5 & 6 GHz with 100 & 200 MHz bandwidth," in *2017 IEEE 28th Annual International Symposium on Personal, Indoor, and Mobile Radio Communications (PIMRC)*, Oct 2017, pp. 1–5.

[8] L. Hao, J. Rodríguez-Piñeiro, X. Yin, and H. Wang, "Measurement-Based Massive MIMO Polarimetric Channel Characterization in Outdoor Environment," *IEEE Access*, vol. 7, pp. 171 285–171 296, 2019.

[9] L. Hao, X. Yin, J. Rodríguez-Piñeiro, B. Ai, and Z. Zhong, "Measurement-based Massive-MIMO Channel Characterization for Outdoor LoS Scenarios," in *2018 IEEE 29th Annual International Symposium on Personal, Indoor and Mobile Radio Communications (PIMRC)*, Sep. 2018, pp. 1–6.

[10] N. Bailey and M. Bartlett, "An introduction to stochastic processes: With special reference to methods and application." *Journal of the Royal Statistical Society. Series A (General)*, vol. 118, p. 484, 01 1955.

[11] X. Yin and X. Cheng, *Propagation channel characterization, parameter estimation, and modeling for wireless communications*. Singapore: Wiley, 2016.

[12] L. Tian, J. Zhang, H. Tan, P. Tang, and G. Liu, "Propagation characteristics of elevation angles and three dimensional fading channel model with angle offset," *China Communications*, vol. 16, no. 9, pp. 62–78, Sep. 2019.

[13] B. H. Fleury, P. Jourdan, and A. Stucki, "High-resolution channel parameter estimation for MIMO applications using the SAGE algorithm," in *2002 International Zurich Seminar on Broadband Communications Access - Transmission - Networking (Cat. No.02TH8599)*, Feb 2002, pp. 30–30.